THE SPECTRAL BIAS OF POLYNOMIAL NEURAL NETWORKS

Anonymous authors
Paper under double-blind review

ABSTRACT

Polynomial neural networks (PNNs) have been recently shown to be particularly effective at solving the tasks of image generation and face recognition, where high-frequency information is critical. Previous studies have revealed that deep neural networks demonstrate a *spectral bias* towards low-frequency functions, which yields faster learning of low-frequency components during training. Inspired by such studies, we conduct a spectral analysis of the Neural Tangent Kernel (NTK) of PNNs. We find that the Π-Net family, i.e., a recently proposed parametrization of PNNs, speeds up the learning of the higher frequencies. In addition, we show that such a theoretical bias is satisfied in practice through extensive experiments. We expect our analysis to provide novel insights into designing architectures and learning frameworks by incorporating multiplicative interactions via polynomials.

1 INTRODUCTION

Deep neural networks (DNNs) have demonstrated remarkable success in different domains [18, 8]. DNNs can approximate complex functions or even datasets with randomized labels arbitrarily well [42, 2], which makes their ability to avoid over-fitting on real data surprising, since it seems to disagree with prior notions of model complexity. This has sparked the interest in investigating the notion of an "implicit bias" in neural network training, which makes them favor low complexity solutions [38, 17, 22].

The spectral analysis of deep networks offers another perspective on this implicit bias. Deep neural networks demonstrate a learning bias towards low frequency functions - i.e. functions that vary globally without local fluctuations are learned faster when training neural networks via gradient descent [32, 41]. The phenomenon, termed as the *spectral bias* of neural networks [32], has also been explored from the perspective of Neural Tangent Kernel (NTK) [20] regime. The eigenvalues of the obtained kernel influence important characteristics such as the approximation properties and rate of learning [7, 34]. For standard two-layer ReLU networks within the NTK regime, the analysis supports the idea of a spectral bias by showing faster error convergence for information in lower frequencies [9].

Apart from DNNs, multiplicative interactions have demonstrated strong empirical performance on image-based applications [39, 40, 3]. Jayakumar et al. [21] highlight how multiplicative interactions, which construct second degree polynomials, can enlarge the hypothesis space and how this reflects as faster learning for certain classes of functions. Polynomial neural networks (PNNs), that express high order polynomial expansions, have demonstrated state-of-the-art performance in the challenging tasks of image generations [24] and face recognition [14]. Both tasks rely on fine-grained details, which correspond to high-frequency information.

To understand the success of PNNs, we conduct a spectral analysis inspired by the spectral analysis on DNNs. We focus on one such instance of polynomial networks called Π-Nets [13], wherein the output is a piece-wise polynomial function of the input obtained via multiplicative layers. The parameters of a Π-Net can be represented as high-order tensors, while polynomial expansions can offer increased representation power [14]. Our main contributions can be summarized as follows:

1. We analyze two-layer polynomial networks in the NTK regime. By studying the spectral properties of the corresponding kernel, we prove a theoretical speed-up in learning higher frequencies

over standard neural networks and validate the hypothesis in the approximate NTK regime, on the task of learning spherical harmonics.

2. Beyond the NTK regime, we demonstrate this enhanced bias of Π-Nets towards higher frequencies in several experimental settings, beginning from synthetic learning tasks and then proceeding to state-of-art networks and standard inverse problems in imaging.

Aside from improving the understanding of polynomials in neural networks, our proposed analysis also sheds new light on the effect of multiplicative interactions in neural networks, prevalent in certain domains of machine learning including vision and natural language processing [25, 6].

2 Related Work

Polynomial neural networks (PNNs): Older works that explore polynomials in the context of neural networks is mainly divided into two categories: 1) self-organizing networks with hard coded features [19], 2) Pi-Sigma networks [36, 30]. In both cases, the polynomial features do not scale well for higher dimensional inputs, and are not used in high-dimensional signals, such as images. More recent works have used the Hadamard product for capturing correlations between different branches of the architecture. The goal of such methods [3, 39, 40, 14] is to construct new architectures that capture higher-order order correlations between the features. This differs from our goal, since we do not aim to construct a new architecture, but rather to analyze the properties of polynomial neural networks through a spectral analysis.

Polynomial activation functions (PAFs): Polynomial activation functions expand (element-wise) each feature to an rth degree, i.e., they assume a (deep) neural network where the element-wise activation functions are r^{th} degree polynomials. This is substantially different from capturing higher-order correlations across input (or feature) elements like PNNs. Theoretical work on over-parametrization [15], expressive power [26] and generalization of shallow nets [31] have emerged for PAFs. Beyond the differences between PAFs and PNNs, the aforementioned works do not conduct a spectral analysis and do not exhibit the benefits of PNNs for learning high-frequency information.

3 Analysis of Polynomial Neural Networks in the NTK regime

In this section, we conduct a careful analysis of the kernel approximation of polynomial neural networks (PNNs) to gain insight on the effect of the multiplicative interactions. PNNs include multiplicative interactions and express high-degree polynomial expansions. The recent parametrization of the Π-Net family [13], which we summarize below, is used as a representative PNN. We review the tangent kernel approximation of neural networks and then we derive the tangent kernel of two-layer Π-Nets. This allows us to conduct a spectral analysis to better understand the approximation properties as well as the spectral bias of Π-Nets.

Notation: We denote by $\langle \cdot, \cdot \rangle$ the standard inner-product on $\mathbb{R}^d$. For two vectors $\mathbf{x}, \mathbf{y} \in \mathbb{R}^d$, $\mathbf{x} * \mathbf{y}$ denotes the element-wise or Hadamard product. We define the asymptotic notations $\Omega(\cdot)$ and $\tilde{\Omega}(\cdot)$ as follows: Let a_n and b_n be two sequences. We write $a_n = \Omega(b_n)$ if $\liminf_{n\to\infty} |a_n/b_n| > 0$. We use $\tilde{\Omega}(\cdot)$ to hide the logarithmic factors in $\Omega(\cdot)$.

3.1 Π-Net Formulation

A polynomial expansion of the input vector $z \in \mathbb{R}^\delta$ can be used to express the output $x \in \mathbb{R}^o$ as an Nth degree polynomial expansion as follows:

$$x = \sum_{n=1}^{N} \left(\boldsymbol{\mathcal{W}}^{[n]} \prod_{j=2}^{n+1} \times_j z \right) + \beta, \tag{1}$$

where $\beta \in \mathbb{R}^o$ and $\left\{ \boldsymbol{\mathcal{W}}^{[n]} \in \mathbb{R}^{o \times \prod_{m=1}^{n} \times_m d} \right\}_{n=1}^{N}$ are the learnable parameters, and $\times_m$ is the mode-m vector product. Since the number of tensor parameters $\boldsymbol{\mathcal{W}}^{[n]}$ grow exponentially with the degree of the polynomial, a coupled tensor decomposition with factor sharing can be used. The idea in Π-Nets is to propose such decompositions that can capture higher order correlations, and can be

implemented in standard deep learning frameworks. One such decomposition expresses the output x using the following recursive formulation:

$$x_n = \left(\boldsymbol{A}_{[n]}^T z\right) * \left(\boldsymbol{S}_{[n]}^T x_{n-1} + \boldsymbol{B}_{[n]}^T \boldsymbol{b}_{[n]}\right), \tag{2}$$

The second term is exactly the recursive form of a standard neural network (without activations) and therefore in practice, Π-Nets simply augment standard neural network with multiplicative interactions via the Hadamard product. While Π-Nets work even without activations, Π-Nets with activations achieve better performance, wherein the output is a piece-wise polynomial. We include more details in the Appendix.

3.2 The Neural Tangent Kernel

Consider the following two-layer ReLU neural network (without bias parameters) with width m that assumes the following form (defined as in [7]):

$$f_{\mathbf{W}}(\mathbf{x}) = \sqrt{\frac{2}{m}} \mathbf{W_2} \sigma(\mathbf{W_1 x}), \tag{3}$$

where $\mathbf{W_1} \in \mathbb{R}^{m \times (d+1)}$, $\mathbf{W_2} \in \mathbb{R}^{1 \times m}$ and we assume inputs $\{\mathbf{x}\}_{i=1}^n$ follow some distribution τ on the unit sphere $\mathbb{S}^d \in \mathbb{R}^{d+1}$; $\sigma(\cdot)$ denotes the element-wise ReLU operator. As the width of the network m goes to infinity, if the weights at initialization $\mathbf{W}^{(0)}$ are independent and each follow the standard normal distribution, the inner product of the network gradient at initialization gives rise to a limiting kernel, namely the *Neural Tangent Kernel* (NTK) [20] κ defined as :

$$\kappa(\mathbf{x}, \mathbf{x}') = \lim_{m \to \infty} \langle \nabla_{\mathbf{W}} f_{\mathbf{W}^{(0)}}(\mathbf{x}), \nabla_{\mathbf{W}} f_{\mathbf{W}^{(0)}}(\mathbf{x}') \rangle. \tag{4}$$

This kernel has been used to characterize the behavior of sufficiently wide networks $f_{\mathbf{W}}$ during training. For instance, if the network is trained to minimize the ℓ_2 loss, then its training dynamics closely track those of kernel regression under κ. This holds in a particular training regime, referred to as "lazy training" [11], where the parameters hardly vary after initialization and the network can be approximated by its first-order Taylor expansion at initialization as:

$$f_{\mathbf{W}}(\mathbf{x}) \approx f_{\mathbf{W}^{(0)}}(\mathbf{x}) + \langle \nabla_{\mathbf{W}} f_{\mathbf{W}^{(0)}}(\mathbf{x}), \mathbf{W} - \mathbf{W}^{(\mathbf{0})} \rangle.$$

In practice however, the conditions of lazy training are often violated (notably, the requirement that the weights do not move) within the first few steps of gradient descent. Nevertheless, the NTK remains a useful theoretical tool for analyzing the neural network behavior as some of its predictions have been shown to hold in practice [9, 28].

The NTK for the two-layer ReLU network (defined in Eq. (3)) takes the following form [7, 11, 16]

$$\boldsymbol{\kappa}(\mathbf{x}, \mathbf{x}') = 2\langle \mathbf{x}, \mathbf{x}' \rangle \kappa_{\mathbf{1}}(\mathbf{x}, \mathbf{x}') + 2\kappa_{\mathbf{2}}(\mathbf{x}, \mathbf{x}'), \tag{5}$$

where the kernels $\kappa_{\mathbf{1}}$ and $\kappa_{\mathbf{2}}$ are defined as follows:

$$\begin{aligned} \kappa_{\mathbf{1}}(\mathbf{x}, \mathbf{x}') &= \mathbf{E}_{\mathbf{w} \sim \mathbf{N}(\mathbf{0}, \mathbf{I})}[\sigma'(\langle \mathbf{w}, \mathbf{x} \rangle)\sigma'(\langle \mathbf{w}, \mathbf{x}' \rangle)], \\ \kappa_{\mathbf{2}}(\mathbf{x}, \mathbf{x}') &= \mathbf{E}_{\mathbf{w} \sim \mathbf{N}(\mathbf{0}, \mathbf{I})}[\sigma(\langle \mathbf{w}, \mathbf{x} \rangle)\sigma(\langle \mathbf{w}, \mathbf{x}' \rangle)], \end{aligned} \tag{6}$$

where $\sigma(\cdot)$ denotes the ReLU operator and $\sigma'(\cdot)$ denotes the indicator function $\mathbf{1}[\cdot \geqslant 0]$. The kernels κ_1, κ_2 have been explicitly computed for the ReLU activation in [33, 12, 7] where they were shown to be positive semi-definite *dot-product* kernels, the function value depends only on the value of the dot-product of the arguments or more formally, $\kappa_1(\mathbf{x}, \mathbf{x}') = g_1(\langle \mathbf{x}, \mathbf{x}' \rangle)$ and $\kappa_2(\mathbf{x}, \mathbf{x}') = g_2(\langle \mathbf{x}, \mathbf{x}' \rangle)$ for some functions $g_1, g_2 : \mathbb{R} \to \mathbb{R}$. These kernels will serve as building blocks for the tangent kernel of the Π-Net architecture studied in the next section.

3.3 Π-Kernel

Here, we derive the tangent kernel for a two-layer Π-Net by supplementing the standard network with a multiplicative interaction layer (via a Hadamard product):

$$f_{\mathbf{W}}(\mathbf{x}) = \sqrt{\frac{2}{m}} \mathbf{W_3}[\sigma(\mathbf{W_2 x}) * \sigma(\mathbf{W_1 x})], \tag{7}$$

where $\mathbf{W_1}, \mathbf{W_2} \in \mathbb{R}^{m \times (d+1)}$, $\mathbf{W_3} \in \mathbb{R}^{1 \times m}$ and we again assume inputs $\{\mathbf{x}\}_{i=1}^n$ that follow some distribution τ on the unit sphere $\mathbb{S}^d \subset \mathbb{R}^{d+1}$. We now present our first main result on the Π-kernel.

Theorem 1 *The limiting kernel for the two-layer* Π*-Net, denoted by* $\kappa_\pi(\mathbf{x}, \mathbf{x}')$*, takes the following form:*

$$\boldsymbol{\kappa_\pi}(\mathbf{x}, \mathbf{x}') = 2(2\langle \mathbf{x}, \mathbf{x}' \rangle \kappa_{\mathbf{1}}(\mathbf{x}, \mathbf{x}') + \kappa_{\mathbf{2}}(\mathbf{x}, \mathbf{x}'))\kappa_{\mathbf{2}}(\mathbf{x}, \mathbf{x}'), \tag{8}$$

where κ_1, κ_2 *are defined as in Eq. (6).*

The proof follows the standard NTK calculations and is presented in the Appendix. Importantly, the addition of a single multiplicative interaction induces a product of kernels form.

Remark 1 The required width that ensures that the two-layer Π-Net does not deviate from the network at initialization (and thus the corresponding NTK is close to the limiting $\boldsymbol{\kappa_\pi}$) is slightly higher than standard networks, by a factor of about $\Omega(\sqrt{\log m})$ and in practice is quite reasonable. We provide a rough sketch of the proof in the Appendix (end of A.2).

Since the Π-kernel $\boldsymbol{\kappa_\pi}$ can be expressed as a sum of products of continuous positive definite dot-product kernels κ_1 and κ_2, it inherits their regularity properties and is itself a Mercer kernel.

3.4 Spectral analysis

To properly characterize the approximation properties and the behavior during training of this newly derived kernel, we study its Mercer decomposition. Indeed, this approach was used in [7] to show that the 2-layer NTK Eq. (5) has better approximation properties than a fixed first layer network, and in [9] to study the spectral bias of feed forward ReLU networks.

The Mercer decomposition of a kernel κ is derived from the eigenvalues and eigenfunction of the integral operator associated to the kernel (see [35] Theorem 2.10 and references therein). Taking $\mathcal{X}$ to be some compact set in $\mathbb{R}^d$, recall that for any continuous kernel function $\kappa : \mathcal{X} \times \mathcal{X} \to \mathbb{R}$ and Borel measure τ on $\mathcal{X}$, we can define an integral operator L_κ that "convolves" any square integrable function $f \in L^2_\tau(\mathcal{X})$ with κ:

$$L_\kappa(f)(\mathbf{x}) = \int_X \kappa(\mathbf{x}, \mathbf{y}) f(\mathbf{y}) d\tau(\mathbf{y}). \tag{9}$$

For a Mercer kernel, this linear operator admits countable, real, non-negative eigenvalues $\{\mu_1, \mu_2, \dots\}$ and the associated eigenfunctions form an orthonormal basis of $L^2_\tau(\mathcal{X})$. If the data is uniform on the sphere $\mathbb{S}^d$, and κ is a dot-product kernel, then these eigenfunctions of L_κ are the spherical harmonics ([37], Lemma 4). Consequently, by applying Mercer's Theorem, we can obtain the following decomposition:

$$\kappa(\mathbf{x}, \mathbf{x}') = \sum_{k=0}^{\infty} \mu_k \sum_{j=1}^{N(d,k)} Y_{k,j}(\mathbf{x}) Y_{k,j}(\mathbf{x}'), \tag{10}$$

where $Y_{k,j}$ for $j = 1, 2 \dots N(d,k)$ represent the spherical harmonics of degree k in $d+1$ variables (whose explicit formula is given in Appendix D.1 in [4]) , and $N(d,k) := \frac{2k+d-1}{k}\binom{k+d-2}{d-1}$.

From this, we can characterize the RKHS $\mathcal{H}$ associated to κ as follows:

$$\mathcal{H} = \left\{ f = \sum_{k \geqslant 0, \mu_k \neq 0} \sum_{j=1}^{N(d,k)} a_{k,j} Y_{k,j}(\cdot) \text{ subject to } \|f\|^2_{\mathcal{H}} = \sum_{k \geqslant 0, \mu_k \neq 0} \sum_{j=1}^{N(d,k)} \frac{a^2_{k,j}}{\mu_k} < \infty \right\}.$$

The benefit of determining the decay rate of the eigenvalues $\{\mu_1, \mu_2, \dots\}$ can be easily deducted from the previous set as the eigenvalues determine the *size* of $\mathcal{H}$. Indeed, the slower the decay of $\{\mu_1, \mu_2, \dots\}$, the more sequences $(a_{k,j})_{k,j}$ will verify $\sum_{k \geqslant 0, \mu_k \neq 0} \sum_{j=1}^{N(d,k)} \frac{a^2_{k,j}}{\mu_k} < \infty$. Moreover, the results of [9] rely on this decay rate to show that gradient descent on wide networks picks up low-frequency information first (Theorem 4.2, [9]). This decay rate is therefore of central importance. Next, we present the prior results on characterizing this decay rate for the kernel obtained for the two-layer feed forward ReLU network (Eq. (5)). From there, we derive the same for the Π-kernel.

Proposition 1 *(Theorem 4.3 in Cao et al. [9], Proposition 5 in Bietti & Mairal [7]) For the tangent kernel corresponding to two-layer feed forward ReLU network, the eigenvalues* $(\mu_k)_k$ *satisfy the*

following:

$$\begin{cases} \mu_0, \mu_1 = \Omega(1), \\ \mu_k = 0, \textit{when } k \textit{ is odd}, \\ \mu_k = \Omega(k^{-d-1}) \textit{ when } k \gg d. \end{cases} \tag{11}$$

The decay is exponentially fast in the input dimension d. For the Π-kernel, we show the following improvement.

Theorem 2 *Let $\{\mu_1^\Pi, \mu_2^\Pi, \dots\}$ denote the eigenvalues of the linear operator $L_{\boldsymbol{\kappa_\pi}}$ associated to the kernel $\boldsymbol{\kappa_\pi}$. Then for $k \gg d$, it holds that*

$$\mu_k^\Pi = \Omega(k^{-d/2-2}).$$

The proof of the theorem is provided in the Appendix. The main idea is to plug in the Mercer decomposition of each kernel, leading to a product of polynomials form. The expansion of this product then allows for isolating the dominant terms contributing to the eigenvalues for each frequency.

The key take-away is the much slower rate of decay the kth eigenvalue (an order almost $\Omega(k^{(d/2)})$) when compared to the standard two-layer NTK. An immediate consequence is a "larger" RKHS, which lends the Π-kernel superior approximation properties in the higher frequencies. Further, when combined with the findings of [9], it yields a speed-up in learning higher frequency harmonics.

Remark 2 On the point of a "larger" RKHS, it is important to note the two perspectives at play. Firstly, as we already commented, is the idea that a slower decay implies more functions contained in the RKHS, leading to better approximation properties. However, from the classical statistical learning point of view, while a larger RKHS makes the optimization problem easier, it can lead to a prediction performance that is sub-optimal [5]. Thus, it eventually relates to the traditional question about finding the optimal trade-off. We will note through our experiments that it is the perspective relating to better approximation properties and optimization for the Π-kernel that dominates.

Remark 3 The $k \gg d$ setting may not reflect the case for image-based applications. For instance, generation tasks wherein the output is an image of resolution $d \times d$, the higher frequencies of interest roughly correspond to the order of $\Omega(d)$. Consequently, the exponential improvement in the decay rate for the $k \gg d$ setting, and by extension in the approximation properties of the RKHS as well as the speed of learning higher frequency information, may not be as dramatic elsewhere. Nevertheless, our analysis provides sufficient intuition to expect a notable degree of improvement in other realistic settings.

In the next section, we put this prediction to the test by extensively examining whether or not Π-nets exhibit a different spectral bias than standard neural networks.

4 Numerical Evidence

The analysis in Section 3 reveals that polynomial neural networks in the NTK regime learn higher frequency information faster. In practice however, neural networks significantly deviate from the near-initialization NTK conditions within just one or two iterations of gradient descent. Therefore, to verify the analysis on the spectral bias of Π-Nets, we conduct a series of experiments that increasingly deviate from the assumptions of the NTK regime, including image-based datasets which further verify our theoretical analysis. We initially describe the experiments on synthetic data (Section 4.1), then move onto realistic settings. For all our experiments, we will use Π-Nets based on the product of polynomials formulation (Appendix), in the same vein as [13].

4.1 Experiments on synthetic data

Our first experiment relates to learning spherical harmonics in approximate infinite width NTK regime [9]. More precisely, the task comprises of learning linear combinations of spherical harmonics with data inputs uniformly distributed on the unit sphere. For this, we consider large-width two-layer networks to simulate the infinite-width settings and we compare the performance of Π-Nets against standard neural networks. The optimization method is vanilla gradient descent with

batch size equal to the number of training samples, to avoid stochastic effects. Our observations align with our theoretical findings, the results are deferred to Appendix due to space constraints. Next, we assess whether the spectral bias manifests beyond the NTK regime.

Learning Sinusoids The goal is to learn sinusoidal signals [32]. Given frequencies $k_i \in \mathcal{K}$, with corresponding amplitudes $A_i \in \alpha$ and phases $\phi_i \in \Phi$, the target map $f^* : [0, 1] \to \mathbb{R}$ is defined as $f^*(x) = A_i \sin(2\pi k_i x + \phi_i)$. We approximate this map with two methods: i) a fully connected neural network and ii) a Π-Net. In the first setting, we compare a 256-unit wide, six-layer deep neural network against a 256-unit wide, six-layer deep Π-Net (which has five multiplicative layers). In each case, the network f_θ (parametrized by θ) regresses over f^* ($\mathcal{K} = (5, 10, ..., 45, 50)$, $\phi_i \sim U(0, 2\pi)$ and $A_i = 1 \; \forall \, i$), using $N = 200$ evenly spaced input samples over $[0, 1]$ and with a fixed learning rate (same for both networks); the spectrum of the network $\tilde{f}_\theta(k)$ is monitored as training progresses and we track the magnitude of learned components for each frequency of interest, averaged it over 5 runs (Fig.1).

Remark 4 The experimental setup for training the two networks replicates the setup of Rahaman et al. [32], without any special initialization or hyper-parameter tuning for either network. As aforementioned, the Π-Net architecture is implemented exactly as the product of polynomials formulation specified in the Appendix.

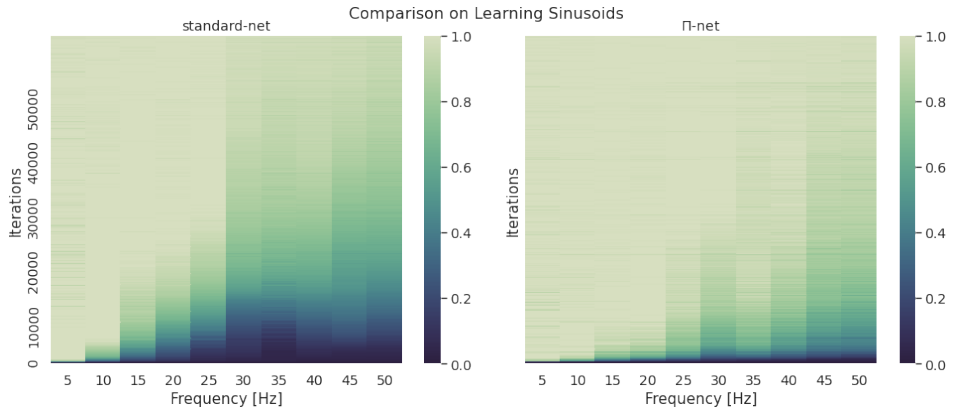

Figure 1: Comparison of learning speeds across different frequencies. The target signal. i.e., sinusoids, is transformed in the Fourier domain and the learned components are compared to the true amplitudes. On the colormap scale, 1 denotes the perfect approximation. We observe that the Π-Net (on the right) acquires information corresponding to higher frequencies faster, i.e., lower in the y axis, than a standard network (on the left).

Due to additional multiplicative layers, Π-Nets have more learnable parameters than standard networks of the same depth. We conduct a second experiment, where we compare a nine-layer feedforward network with a six-layer Π-Net with only three multiplicative layers, such that the feedforward network includes more parameters. We observe that while depth does help improve the learning speeds for higher frequencies, it is not as effective as the multiplicative layers in Π-Nets (Fig. 2).

Skip connections (additive) in deeper networks are known to speed-up training. To disentangle this effect from multiplicative skip connections, we consider an alternate experiment in the Appendix where we train a Π-Net and compare it with a standard network with the same architecture, but with additive skip connections instead of multiplicative. We verify that the improvement in the speed of learning higher frequencies can not be achieved using trivial additive skip connections.

Robustness to Perturbations: Motivated by the observations of Rahaman et al. [32], we evaluate the susceptibility of higher frequencies to random perturbations for standard networks and Π-Nets. The setup relies on the learning task in the previous experiment. More precisely, following convergence of the network to a low-error approximation of target f^* (denoted by $f_{\theta*}$), random isotropic perturbations are introduced to the network parameters: $\theta = \theta^* + \delta\hat{\theta}$. We monitor the effect of increasing the perturbation magnitude δ on the frequencies of interest. In the first setting (Fig. 3), we compare the effects of perturbations on the six-layer standard network to the six-layer Π-Net

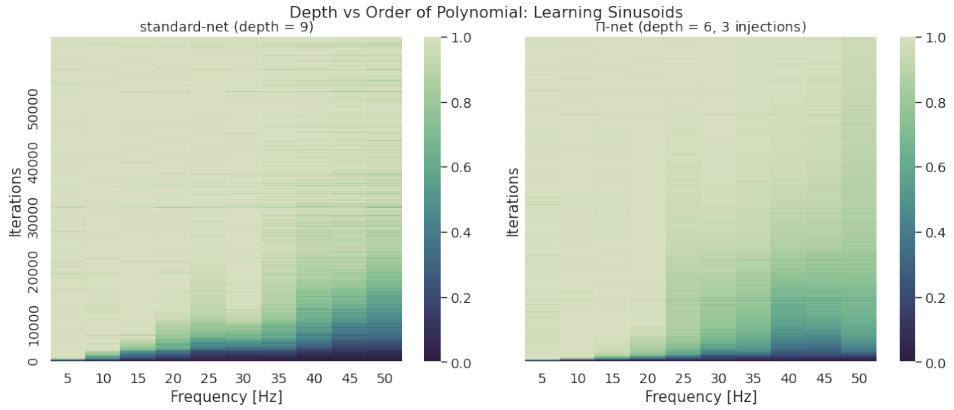

Figure 2: The heat map denotes a comparison on the effectiveness of increasing depth vs introducing multiplicative interactions via Π-Nets for learning high-frequency information. The empirical evidence shows that multiplicative layers are more effective for learning higher frequencies faster.

(with five multiplicative injections). In the second setting, we directly compare the two variants of 6-layer deep Π-Nets i.e. one with five injections and the other with three injections, the results are deferred to the Appendix.

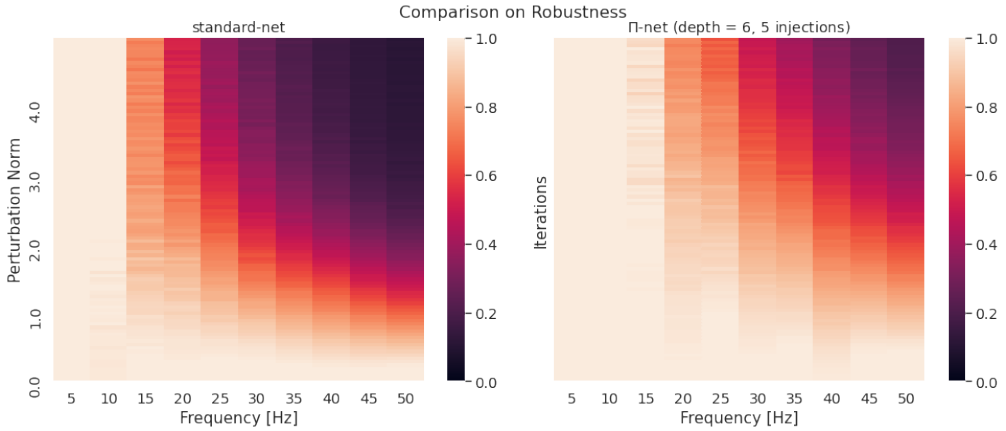

Figure 3: The heap maps present a comparison on the robustness to random parameter perturbations for six-layer standard vs six-layer Π-Net. The y-axis denotes the norm of the random perturbation. For standard networks, the high-frequency information is lost quickly as the perturbation norm increases, while Π-Nets are much more effective at retaining higher frequency information, even under large perturbations.

Discussion: In the task of learning sinusoids, multiplicative interactions speed up the learning of higher frequency sinusoids. Additionally, they are more effective at doing so than simply increasing the depth of the network. Through the robustness experiment, we see that Π-Nets are more robust to perturbations in the higher frequencies. Remarkably, the Π-Net with more interactions is noticeably more robust than the lower degree polynomial network (Fig. 12 in the appendix). We hypothesize that Π-Nets enhance the representational space for higher frequencies, relating to our observations on the RKHS in the NTK regime, which makes them less susceptible than standard neural networks. This could also explain why more multiplicative 'injections' lead to more robustness.

4.2 Learning Images

We observed that multiplicative injections allowed fully connected networks to pick up higher frequency information faster. On the other hand, Deep Convolutional Neural Networks (DCNNs [27])

are more ubiquitous in computer vision, partly due to the DCNN structure imposing a suitable prior for tasks with natural images, termed as the Deep Image Prior (DIP) [29]. Therefore, we check how this prior changes with multiplicative interactions in Π-Nets. We adapt the denoising setup from the DIP framework.

Experiment - Denoising: We consider an image $x \in \mathbb{R}^{3\times H\times W}$ and obtain its noisy version $x_0 = x + \delta$, perturbed with Gaussian noise. For the input, we sample a random tensor $z \in \mathbb{R}^{N\times H\times W}$ (N = 32 in our setup). We consider a neural network f_θ (making the parametrization by θ explicit), and optimize the following objective:

$$\min_{\theta} ||f_\theta(z) - x_0||^2. \tag{12}$$

We expect the DCNN structure to first learn the ("natural") features corresponding to the true image x and pick up the noise only in the latter stages, which can then be avoided using early-stopping.

Remark 5 Our goal in this experiment is not to look at the denoising performance. Instead, our primary goal is to validate the experimental observation on sinusoids and assess whether Π-Nets can speed up learning of high frequencies in real-world applications. If the speed up is confirmed, Π-Nets can be early-stopped, i.e., require less iterations for achieving the target result.

As in [32], we experiment with the U-net architecture, adapting it suitably for Π-Nets. The implementation details are included in the Appendix. We train both networks for 2500 iterations, with the same learning rate and identical input tensor z. We monitor the Peak Signal-to-Noise Ratio (PSNR) curves while training, in Fig. 4. The peak-PSNR with the true image for both standard and Π-Nets are roughly the same, indicating similar denoising performance. However, Π-net achieves this peak PSNR in approximately half the number of iterations. Beyond this point, the Π-net PSNR with the true image decreases as it starts to pick up the high-frequency noise. We confirm this in the visual snapshot of the output of the two networks (Fig. 15 in the appendix). We conclude that Π-Nets do indeed speed up learning in images, by showing a reduced impedance towards high-frequency information. Next, we check how this bias affects learning high frequency information pertaining to natural images in the absence of noise.

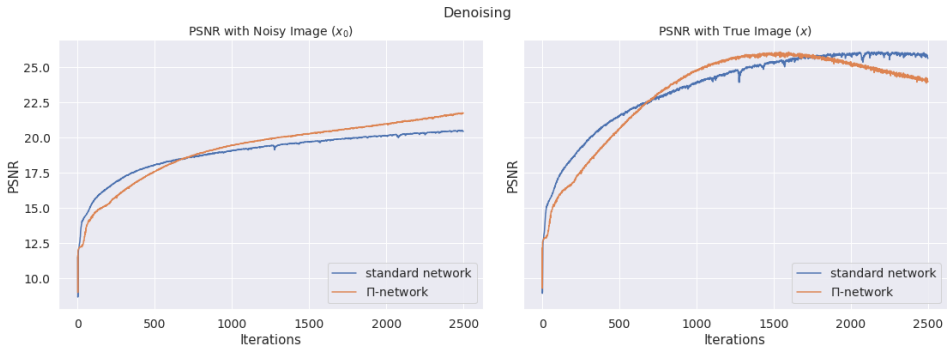

Figure 4: The plots track the progress of the denoising task in the DIP setup via measuring the PSNR w.r.t. the noisy image (left) and the true image (right). We ideally want to stop the optimization process when the PSNR w.r.t the true image is maximum. We observe that for Π-Nets, the maximum PSNR point occurs much earlier, beyond which the PSNR w.r.t the true image starts to decrease as the network begins to learn the noise. This indicates that the Π-Net shows a reduced impedance towards high frequency information, compared to standard networks.

Experiment - Power Spectrum Analysis: We consider the identical setup as the denoising experiment but without the noise perturbation, setting $\delta = \mathbf{0}$. Therefore, the task for the network f_θ learn θ^* such that $f_{\theta*}(z) = x$. We allow 600 iterations of gradient descent and we monitor the radial power spectral density (p.s.d.) of the network output image against the ground truth p.s.d. It allows us to explicitly track the learning progress for each the frequency magnitude.

We use the same U-net structure and suitably modify it for Π-Nets as before. Since the multiplicative interactions introduce more parameters, we reduce the depth/scale (by scale, we mean number of down/up-sampling operations in the U-net) of Π-Net to ensure roughly the same parameters (∼1.3

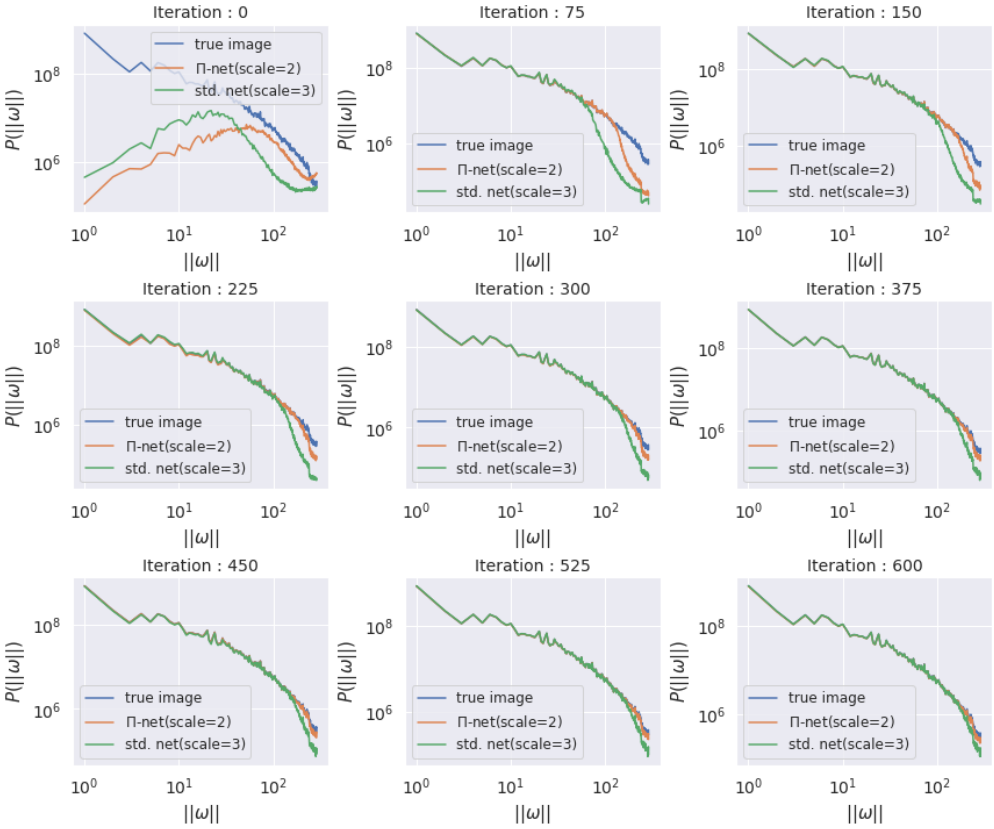

Figure 5: We compare the power spectral density curves at different checkpoints during 600 iterations of optimization, for standard (scale = 3) vs Π networks (scale = 2). The goal for each network is to match the power spectral density of the target image. We observe that the Π-Net picks up high-frequency information in the image faster.

million). The learning speeds in different frequencies can be observed in Fig. 5. In the Appendix, we repeat the same experiment for equal depth networks.

Discussion: From the preceding two experiments, we establish that Π-Nets retain their superiority in picking up high frequency information for larger DCNNs. In the Appendix, we note the effect of multiplicative interactions on the deep image prior of the network. We also verify that this altered spectral bias remains relevant for standard learning tasks with natural images. Consequently, for tasks where capturing the finer details of the image is important (such as the denoising instance above), this potentially leads to a reduced training time for Π-Nets as compared to standard networks.

5 Discussion

In this work, we focus on the spectral of polynomial neural networks. Our theoretical results in the NTK regime utilize a two-layer polynomial network and demonstrate a speed-up in the learning of higher frequencies over standard neural networks. We experimentally verify these properties, even outside of the NTK training regime. Our theoretical results also offer intuition behind the success of networks that use multiplicative interactions, such as StyleGAN [24], whose connections to polynomials have been noted previously [14]. In the future, we intend to study the performance of polynomial and multiplicative interactions in state-of-the-art conditional generative models, such as in image generation or deblurring, where high-frequency information is critical for photo-realistic outcome. In addition, we intend to explore whether the spectral bias of polynomials translates to differences in their generalization properties.

REFERENCES

[1] Zeyuan Allen-Zhu, Yuanzhi Li, and Zhao Song. A convergence theory for deep learning via over-parameterization. *CoRR*, abs/1811.03962, 2018. URL http://arxiv.org/abs/1811.03962.

[2] Devansh Arpit, Stanisław Jastrzebski, Nicolas Ballas, David Krueger, Emmanuel Bengio, Maxinder S. Kanwal, Tegan Maharaj, Asja Fischer, Aaron Courville, Yoshua Bengio, and Simon Lacoste-Julien. A closer look at memorization in deep networks. *arXiv:1706.05394 [cs, stat]*, July 2017. URL http://arxiv.org/abs/1706.05394. arXiv: 1706.05394.

[3] Francesca Babiloni, Ioannis Marras, Filippos Kokkinos, Jiankang Deng, Grigorios Chrysos, and Stefanos Zafeiriou. Poly-nl: Linear complexity non-local layers with polynomials. In *International Conference on Computer Vision (ICCV)*, 2021.

[4] Francis Bach. Breaking the Curse of Dimensionality with Convex Neural Networks. *arXiv:1412.8690 [cs, math, stat]*, October 2016. URL http://arxiv.org/abs/1412.8690. arXiv: 1412.8690.

[5] Francis R. Bach. Sharp analysis of low-rank kernel matrix approximations. *CoRR*, abs/1208.2015, 2012. URL http://arxiv.org/abs/1208.2015.

[6] Dzmitry Bahdanau, Kyunghyun Cho, and Yoshua Bengio. Neural Machine Translation by Jointly Learning to Align and Translate. *arXiv:1409.0473 [cs, stat]*, May 2016. URL http://arxiv.org/abs/1409.0473. arXiv: 1409.0473.

[7] Alberto Bietti and Julien Mairal. On the Inductive Bias of Neural Tangent Kernels. *arXiv:1905.12173 [cs, stat]*, October 2019. URL http://arxiv.org/abs/1905.12173. arXiv: 1905.12173.

[8] Tom B. Brown, Benjamin Mann, Nick Ryder, Melanie Subbiah, Jared Kaplan, Prafulla Dhariwal, Arvind Neelakantan, Pranav Shyam, Girish Sastry, Amanda Askell, Sandhini Agarwal, Ariel Herbert-Voss, Gretchen Krueger, Tom Henighan, Rewon Child, Aditya Ramesh, Daniel M. Ziegler, Jeffrey Wu, Clemens Winter, Christopher Hesse, Mark Chen, Eric Sigler, Mateusz Litwin, Scott Gray, Benjamin Chess, Jack Clark, Christopher Berner, Sam McCandlish, Alec Radford, Ilya Sutskever, and Dario Amodei. Language Models are Few-Shot Learners. *arXiv:2005.14165 [cs]*, July 2020. URL http://arxiv.org/abs/2005.14165. arXiv: 2005.14165.

[9] Yuan Cao, Zhiying Fang, Yue Wu, Ding-Xuan Zhou, and Quanquan Gu. Towards Understanding the Spectral Bias of Deep Learning. *arXiv:1912.01198 [cs, stat]*, October 2020. URL http://arxiv.org/abs/1912.01198. arXiv: 1912.01198.

[10] L. Carlitz. The product of two ultraspherical polynomials. *Glasgow Mathematical Journal*, 5(2):76–79, July 1961. ISSN 2051-2104, 2040-6185. doi: 10.1017/S204061850003433X. URL https://www.cambridge.org/core/journals/glasgow-mathematical-journal/article/product-of-two-ultraspherical-polynomials/BF734D19E2D88047AFD196033D20766A. Publisher: Cambridge University Press.

[11] Lenaic Chizat, Edouard Oyallon, and Francis Bach. On Lazy Training in Differentiable Programming. *arXiv:1812.07956 [cs, math]*, January 2020. URL http://arxiv.org/abs/1812.07956. arXiv: 1812.07956.

[12] Youngmin Cho and Lawrence Saul. Kernel Methods for Deep Learning. In *Advances in Neural Information Processing Systems*, volume 22. Curran Associates, Inc., 2009. URL https://papers.nips.cc/paper/2009/hash/5751ec3e9a4feab575962e78e006250d-Abstract.html.

[13] Grigorios G. Chrysos, Stylianos Moschoglou, Giorgos Bouritsas, Yannis Panagakis, Jiankang Deng, and Stefanos Zafeiriou. P-nets: Deep Polynomial Neural Networks. pp. 7325–7335, 2020. URL https://openaccess.thecvf.com/content_CVPR_2020/html/Chrysos_P-nets_Deep_Polynomial_Neural_Networks_CVPR_2020_paper.html.

[14] Grigorios G. Chrysos, Stylianos Moschoglou, Giorgos Bouritsas, Jiankang Deng, Yannis Panagakis, and Stefanos P Zafeiriou. Deep Polynomial Neural Networks. pp. 1–1, 2021. ISSN 1939-3539. doi: 10.1109/TPAMI.2021.3058891. Conference Name: IEEE Transactions on Pattern Analysis and Machine Intelligence.

[15] Simon Du and Jason Lee. On the power of over-parametrization in neural networks with quadratic activation. In *International Conference on Machine Learning (ICML)*, pp. 1329–1338, 2018.

[16] Simon S. Du, Xiyu Zhai, Barnabas Poczos, and Aarti Singh. Gradient Descent Provably Optimizes Over-parameterized Neural Networks. *arXiv:1810.02054 [cs, math, stat]*, February 2019. URL http://arxiv.org/abs/1810.02054. arXiv: 1810.02054.

[17] Suriya Gunasekar, Jason D Lee, Daniel Soudry, and Nati Srebro. Implicit Bias of Gradient Descent on Linear Convolutional Networks. In *Advances in Neural Information Processing Systems*, volume 31. Curran Associates, Inc., 2018. URL https://proceedings.neurips.cc/paper/2018/hash/0e98aeeb54acf612b9eb4e48a269814c-Abstract.html.

[18] Yanping Huang, Youlong Cheng, Ankur Bapna, Orhan Firat, Mia Xu Chen, Dehao Chen, HyoukJoong Lee, Jiquan Ngiam, Quoc V. Le, Yonghui Wu, and Zhifeng Chen. GPipe: Efficient Training of Giant Neural Networks using Pipeline Parallelism. *arXiv:1811.06965 [cs]*, July 2019. URL http://arxiv.org/abs/1811.06965. arXiv: 1811.06965.

[19] A. G. Ivakhnenko. Polynomial Theory of Complex Systems. *IEEE Transactions on Systems, Man, and Cybernetics*, SMC-1(4):364–378, October 1971. ISSN 2168-2909. doi: 10.1109/TSMC.1971.4308320. Conference Name: IEEE Transactions on Systems, Man, and Cybernetics.

[20] Arthur Jacot, Franck Gabriel, and Clément Hongler. Neural Tangent Kernel: Convergence and Generalization in Neural Networks. *arXiv:1806.07572 [cs, math, stat]*, February 2020. URL http://arxiv.org/abs/1806.07572. arXiv: 1806.07572.

[21] Siddhant M. Jayakumar, Wojciech M. Czarnecki, Jacob Menick, Jonathan Schwarz, Jack Rae, Simon Osindero, Yee Whye Teh, Tim Harley, and Razvan Pascanu. Multiplicative interactions and where to find them. In *International Conference on Learning Representations (ICLR)*, 2020.

[22] Ziwei Ji and Matus Telgarsky. The implicit bias of gradient descent on nonseparable data. In *Proceedings of the Thirty-Second Conference on Learning Theory*, pp. 1772–1798. PMLR, June 2019. URL https://proceedings.mlr.press/v99/ji19a.html. ISSN: 2640-3498.

[23] Ziwei Ji, Justin D. Li, and Matus Telgarsky. Early-stopped neural networks are consistent. 2021. arXiv:2106.05932 [cs.LG].

[24] Tero Karras, Samuli Laine, and Timo Aila. A style-based generator architecture for generative adversarial networks. In *Conference on Computer Vision and Pattern Recognition (CVPR)*, 2019.

[25] Tero Karras, Samuli Laine, and Timo Aila. A Style-Based Generator Architecture for Generative Adversarial Networks. *arXiv:1812.04948 [cs, stat]*, March 2019. URL http://arxiv.org/abs/1812.04948. arXiv: 1812.04948.

[26] Joe Kileel, Matthew Trager, and Joan Bruna. On the expressive power of deep polynomial neural networks. *Advances in neural information processing systems (NeurIPS)*, 32:10310–10319, 2019.

[27] Yann LeCun and Yoshua Bengio. Convolutional networks for images, speech, and time series. In *The handbook of brain theory and neural networks*, pp. 255–258. MIT Press, Cambridge, MA, USA, October 1998. ISBN 978-0-262-51102-5.

[28] Jaehoon Lee, Lechao Xiao, Samuel Schoenholz, Yasaman Bahri, Roman Novak, Jascha Sohl-Dickstein, and Jeffrey Pennington. Wide neural networks of any depth evolve as linear models under gradient descent. *Advances in neural information processing systems*, 32:8572–8583, 2019.

[29] Victor Lempitsky, Andrea Vedaldi, and Dmitry Ulyanov. Deep Image Prior. In *2018 IEEE/CVF Conference on Computer Vision and Pattern Recognition*, pp. 9446–9454, June 2018. doi: 10.1109/CVPR.2018.00984. ISSN: 2575-7075.

[30] Chien-Kuo Li. A Sigma-Pi-Sigma Neural Network (SPSNN). *Neural Processing Letters*, 17 (1):1–19, February 2003. ISSN 1573-773X. doi: 10.1023/A:1022967523886. URL https://doi.org/10.1023/A:1022967523886.

[31] Stefano Sarao Mannelli, Eric Vanden-Eijnden, and Lenka Zdeborová. Optimization and generalization of shallow neural networks with quadratic activation functions. *arXiv preprint arXiv:2006.15459*, 2020.

[32] Nasim Rahaman, Aristide Baratin, Devansh Arpit, Felix Draxler, Min Lin, Fred A. Hamprecht, Yoshua Bengio, and Aaron Courville. On the Spectral Bias of Neural Networks. *arXiv:1806.08734 [cs, stat]*, May 2019. URL http://arxiv.org/abs/1806.08734.

[33] Nicolas Le Roux and Yoshua Bengio. Continuous neural networks. In Marina Meila and Xiaotong Shen (eds.), *Proceedings of the Eleventh International Conference on Artificial Intelligence and Statistics*, volume 2 of *Proceedings of Machine Learning Research*, pp. 404–411, San Juan, Puerto Rico, 21–24 Mar 2007. PMLR. URL https://proceedings.mlr.press/v2/leroux07a.html.

[34] Meyer Scetbon and Zaid Harchaoui. A spectral analysis of dot-product kernels, 2021.

[35] Bernhard Schölkopf, Alexander J Smola, Francis Bach, et al. *Learning with kernels: support vector machines, regularization, optimization, and beyond*. MIT press, 2002.

[36] Y. Shin and J. Ghosh. The pi-sigma network: an efficient higher-order neural network for pattern classification and function approximation. In *IJCNN-91-Seattle International Joint Conference on Neural Networks*, volume i, pp. 13–18 vol.1, July 1991. doi: 10.1109/IJCNN.1991.155142.

[37] Alex Smola, Zoltán Óvári, and Robert C Williamson. Regularization with dot-product kernels. In T. Leen, T. Dietterich, and V. Tresp (eds.), *Advances in Neural Information Processing Systems*, volume 13. MIT Press, 2001. URL https://proceedings.neurips.cc/paper/2000/file/d25414405eb37dae1c14b18d6a2cac34-Paper.pdf.

[38] Daniel Soudry, Elad Hoffer, Mor Shpigel Nacson, Suriya Gunasekar, and Nathan Srebro. The Implicit Bias of Gradient Descent on Separable Data. *arXiv:1710.10345 [cs, stat]*, December 2018. URL http://arxiv.org/abs/1710.10345. arXiv: 1710.10345.

[39] Rupesh Kumar Srivastava, Klaus Greff, and Jürgen Schmidhuber. Highway Networks. *arXiv:1505.00387 [cs]*, November 2015. URL http://arxiv.org/abs/1505.00387. arXiv: 1505.00387.

[40] Yan Wang, Lingxi Xie, Chenxi Liu, Siyuan Qiao, Ya Zhang, Wenjun Zhang, Qi Tian, and Alan Yuille. Sort: Second-order response transform for visual recognition. In *International Conference on Computer Vision (ICCV)*, pp. 1359–1368, 2017.

[41] Zhi-Qin John Xu, Yaoyu Zhang, Tao Luo, Yanyang Xiao, and Zheng Ma. Frequency principle: Fourier analysis sheds light on deep neural networks. *CoRR*, abs/1901.06523, 2019. URL http://arxiv.org/abs/1901.06523.

[42] Chiyuan Zhang, Samy Bengio, Moritz Hardt, Benjamin Recht, and Oriol Vinyals. Understanding deep learning requires rethinking generalization. *arXiv:1611.03530 [cs]*, February 2017. URL http://arxiv.org/abs/1611.03530. arXiv: 1611.03530.

A APPENDIX

A.1 A PRIMER ON POLYNOMIAL NEURAL NETWORKS (Π-NETS)

Polynomial neural networks (Π-Nets) [13] were recently introduced with the output being a high degree polynomial expansion of the input. The parameters of Π-Nets can be represented as higher order tensors. These networks are able to serve as function approximators even without the use of non-linear activations. When used in conjunction with activations, the models demonstrate better expressivity and achieve state-of-art results on a variety of learning tasks. We next describe the construction of Π-Nets.

A.1.1 METHOD

Π-Net learns a function $G : \mathbb{R}^d \rightarrow \mathbb{R}^o$, such that each element of the output x_j can be expressed as a polynomial of all the input elements z_i, with $i \in [1, d]$ as follows:

$$\begin{aligned} x_j = G(\boldsymbol{z})_j = \beta_j + {\boldsymbol{w}_j^{[1]}}^T \boldsymbol{z} + \boldsymbol{z}^T \boldsymbol{W}_j^{[2]} \boldsymbol{z} + \\ \boldsymbol{\mathcal{W}}_j^{[3]} \times_1 \boldsymbol{z} \times_2 \boldsymbol{z} \times_3 \boldsymbol{z} + \cdots + \boldsymbol{\mathcal{W}}_j^{[N]} \prod_{n=1}^{N} \times_n \boldsymbol{z}, \end{aligned} \tag{13}$$

where $\beta_j \in \mathbb{R}$ and $\left\{\boldsymbol{\mathcal{W}}_j^{[n]} \in \mathbb{R}^{\prod_{m=1}^{n} \times_m d}\right\}_{n=1}^{N}$ are parameters for approximating the output x_j. The correlations (of the input elements z_i) up to N^{th} order emerge in Eq. (13). More compactly:

$$\boldsymbol{x} = G(z) = \sum_{n=1}^{N} \left(\boldsymbol{\mathcal{W}}^{[n]} \prod_{j=2}^{n+1} \times_j \boldsymbol{z} \right) + \beta, \tag{14}$$

where $\beta \in \mathbb{R}^o$ and $\left\{\boldsymbol{\mathcal{W}}^{[n]} \in \mathbb{R}^{o \times \prod_{m=1}^{n} \times_m d}\right\}_{n=1}^{N}$ are the learnable parameters. This form allows us to approximate any smooth function as per an extension of the Weierstrass Theorem. To prevent an exponential number of parameters, the authors propose using coupled tensor decompositions.

A.1.2 TENSOR DECOMPOSITION FOR SINGLE POLYNOMIAL

An appropriate tensor decomposition on the parameters in Eq. (14) allows for implementation with a neural network. Here, we briefly describe one such decomposition:

Model: NCP: Next, we consider a joint hierarchical decomposition on the polynomial parameters. A Nested coupled CP decomposition (NCP) results in the following recursive relationship for N^{th} order approximation:

$$\boldsymbol{x}_n = \left(\boldsymbol{A}_{[n]}^T \boldsymbol{z}\right) * \left(\boldsymbol{S}_{[n]}^T \boldsymbol{x}_{n-1} + \boldsymbol{B}_{[n]}^T \boldsymbol{b}_{[n]}\right), \tag{15}$$

for $n = 2, \ldots, N$ with $\boldsymbol{x}_1 = \left(\boldsymbol{A}_{[n]}^T \boldsymbol{z}\right) * \left(\boldsymbol{B}_{[n]}^T \boldsymbol{b}_{[n]}\right)$ and $\boldsymbol{x} = \boldsymbol{C}\boldsymbol{x}_N + \boldsymbol{\beta}$. The parameters $\boldsymbol{C} \in \mathbb{R}^{o \times k}, \boldsymbol{A}_{[n]} \in \mathbb{R}^{d \times k}, \boldsymbol{S}_{[n]} \in \mathbb{R}^{k \times k}, \boldsymbol{B}_{[n]} \in \mathbb{R}^{\omega \times k}$, $\boldsymbol{b}_{[n]} \in \mathbb{R}^{\omega}$ for $n = 1, \ldots, N$, are learnable. $\left\{\boldsymbol{b}_{[n]} \in \mathbb{R}^{\omega}\right\}_{n=1}^{N}$act as a scaling factor for each parameter tensor, whose role is illustrated in case of the third order approximation in eq.16:

$$G(\boldsymbol{z}) = \boldsymbol{\beta} + \boldsymbol{\mathcal{W}}^{[1]} \times_2 \boldsymbol{b}_{[1]} \times_3 \boldsymbol{z} + \boldsymbol{\mathcal{W}}^{[2]} \times_2 \boldsymbol{b}_{[2]} \times_3 \boldsymbol{z} \times_4 \boldsymbol{z} + \boldsymbol{\mathcal{W}}^{[3]} \times_2 \boldsymbol{b}_{[3]} \times_3 \boldsymbol{z} \times_4 \boldsymbol{z} \times_5 \boldsymbol{z}. \tag{16}$$

Further, the joint factorization of the parameter tensors (in matrix form) for the third order NCP polynomial may be summarized as follows:

- First order parameters : $\boldsymbol{W}_{(1)}^{[1]} = \boldsymbol{C}(\boldsymbol{A}_{[3]} \odot \boldsymbol{B}_{[3]})^T$.

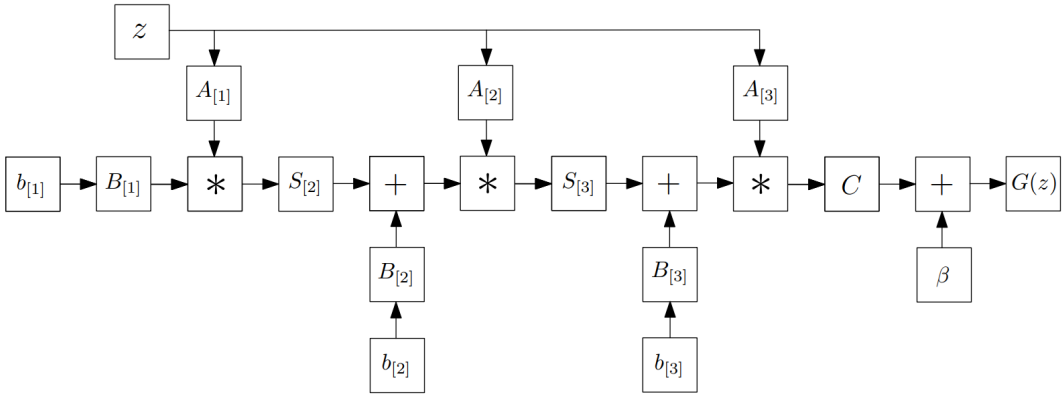

Figure 6: Schematic illustration of the NCP [13].

- Second order parametes: $\boldsymbol{W}_{(1)}^{[2]} = \boldsymbol{C}\left\{\boldsymbol{A}_{[3]} \odot \left[\left(\boldsymbol{A}_{[2]} \odot \boldsymbol{B}_{[2]}\right)\boldsymbol{S}_{[3]}\right]\right\}^T$.
- Third order parameters: $\boldsymbol{W}_{(1)}^{[3]} = \boldsymbol{C}\left\{\boldsymbol{A}_{[3]} \odot \left[\left(\boldsymbol{A}_{[2]} \odot \left\{\left(\boldsymbol{A}_{[1]} \odot \boldsymbol{B}_{[1]}\right)\boldsymbol{S}_{[2]}\right\}\right)\boldsymbol{S}_{[3]}\right]\right\}^T$

A.1.3 Product of Polynomials

The second scheme of implementation approximates the target function using a product of polynomials form, wherein the output of first polynomial is fed to the next and so on. The concept is visually depicted in 7; for instance, if each polynomial is degree two, then stacking N such polynomials results in an overall order of 2^N.

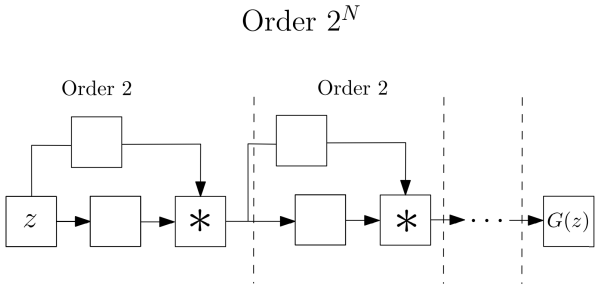

Figure 7: Schematic illustration of the product of polynomials model [13].

Remark: In practice, each matrix operation in the recursive formulation of Π-Nets represents an affine transform on a vector. Therefore, the implementation in standard libraries may be as simple as using a convolutional or a fully-connected layer. The other difference arises due to the multiplicative layers, which may be seen as special 'skip' connections which are combined with the network output via the element-wise vector product (Hadamard product), as opposed to addition. Therefore, it is easy to see why these networks scale as well as standard deep networks.

A.2 PROOF OF THEOREM 1: DERIVING THE Π-KERNEL

In this section, we prove our first main result for the Π-kernel corresponding to theorem 1. Consider a two-layer Π-Net $f_{\mathbf{W}}$ parametrized as follows :

$$f_{\mathbf{W}}(\mathbf{x}) = \sqrt{\frac{2}{m}}\mathbf{W_3}[\sigma(\mathbf{W_2}\mathbf{x}) * \sigma(\mathbf{W_1}\mathbf{x})], \tag{17}$$

where the weights $\mathbf{W_1} \in \mathbb{R}^{m\times d}, \mathbf{W_2} \in \mathbb{R}^{m\times d}, \mathbf{W_3} \in \mathbb{R}^{1\times m}$ are initialized with independent identically distributed $\mathcal{N}(0,1)$ coordinates.

Recall that the neural tangent kernel κ_π corresponds to the limit of the following inner product

$$\kappa_\pi(\mathbf{x},\mathbf{x}') = \lim_{m\to\infty}\langle \nabla_{\mathbf{W}} f_{\mathbf{W}^{(0)}}(\mathbf{x}), \nabla_{\mathbf{W}} f_{\mathbf{W}^{(0)}}(\mathbf{x}')\rangle. \tag{18}$$

We can compute the inner-product Eq. (18) by computing the derivatives with respect to $\mathbf{W_1}$, $\mathbf{W_2}$, $\mathbf{W_3}$ of $f_{\mathbf{W}}$ separately and sum up the inner products to obtain κ_π, since the gradient can be split into three blocks.

We denote by $\tilde{\alpha} := \mathbf{W}_1\mathbf{x}$, and by $\tilde{\beta} := \mathbf{W}_2\mathbf{x}$ the pre-activation vectors; and by α, β the post-activation vectors where the element-wise activation σ is applied to $\tilde{\alpha}$ and $\tilde{\beta}$ respectively.

First consider the derivative w.r.t $\mathbf{W_1}$ denoted $\partial_{\mathbf{W}_1}$:

$$\partial_{W_1}\mathbf{f}_{\mathbf{W}}(\mathbf{x}) = \sqrt{\frac{2}{m}}\sum_{i=1}^{m}\partial_{W_1}\tilde{\alpha}_i(\mathbf{x})\sigma'(\tilde{\alpha}_i(\mathbf{x}))\sigma(\tilde{\beta}_i(\mathbf{x}))\mathbf{W}_3^i. \tag{19}$$

The contribution to the NTK (Eq. (18)) therefore corresponds to $\langle \partial_{W_1}\mathbf{f}_{\mathbf{W}}(\mathbf{x}), \partial_{\mathbf{W}_1}\mathbf{f}_{\mathbf{W}}(\mathbf{x}')\rangle$. Note that since the network is symmetric in $\{\mathbf{W}_1, \mathbf{W}_2\}$, we need only look at $\mathbf{W}_1$ to obtain the contribution for $\mathbf{W}_2$ as well. We find that

$$\begin{aligned}
\langle \partial_{W_1}\mathbf{f}_{\mathbf{W}}(\mathbf{x}), \partial_{\mathbf{W}_1}\mathbf{f}_{\mathbf{W}}(\mathbf{x}')\rangle &= \frac{2}{m}\sum_{i,j=1}^{m}[\partial_{\mathbf{W}_1}\tilde{\alpha}_i(\mathbf{x})\partial_{\mathbf{W}_1}\tilde{\alpha}_j(\mathbf{x}')][\sigma'(\tilde{\alpha}_i(\mathbf{x}))\sigma'(\tilde{\alpha}_j(\mathbf{x}'))][\sigma(\tilde{\beta}_i(\mathbf{x}))\sigma(\tilde{\beta}_j(\mathbf{x}'))]\mathbf{W}_3^i\mathbf{W}_3^j \\
&= \frac{2}{m}\sum_{i,j=1}^{m}[\mathbf{x}^T\mathbf{x}'\delta_{ij}][\sigma'(\tilde{\alpha}_i(\mathbf{x}))\sigma'(\tilde{\alpha}_j(\mathbf{x}'))][\sigma(\tilde{\beta}_i(\mathbf{x}))\sigma(\tilde{\beta}_j(\mathbf{x}'))]\mathbf{W}_3^i\mathbf{W}_3^j \\
&= \frac{2}{m}\sum_{i}^{m}[\mathbf{x}^T\mathbf{x}'\delta_{ii}][\sigma'(\langle\mathbf{W}_1^i,\mathbf{x}\rangle))\sigma'(\langle\mathbf{W}_1^i,\mathbf{x}'\rangle)][\sigma(\langle\mathbf{W}_2^i,\mathbf{x}\rangle))\sigma(\langle W_2^i,\mathbf{x}'\rangle)]\mathbf{W}_3^i\mathbf{W}_3^i.
\end{aligned} \tag{20}$$

As $\lim m \to \infty$, the above quantity converges to its expectation by the law of large numbers because the terms are independent and identically distributed with finite expectation. Consequently,

$$\begin{aligned}
&\lim_{m\to\infty}\langle \partial_{W_1}\mathbf{f}_{\mathbf{W}}(\mathbf{x}), \partial_{\mathbf{W}_1}\mathbf{f}_{\mathbf{W}}(\mathbf{x}')\rangle \\
&= 2\mathbf{x}^T\mathbf{x}'\mathbf{E}_{\mathbf{W}_1,\mathbf{W}_2,\mathbf{W}_3\sim\mathbf{N(0,I)}}\{[\sigma'(\langle\mathbf{W}_1,\mathbf{x}\rangle))\sigma'(\langle\mathbf{W}_1,\mathbf{x}'\rangle)][\sigma(\langle\mathbf{W}_2,\mathbf{x}\rangle))\sigma(\langle\mathbf{W}_2,\mathbf{x}'\rangle)]\mathbf{W}_3^i\mathbf{W}_3^i\} \\
&= 2\mathbf{x}^T\mathbf{x}'\mathbf{E}_{\mathbf{W}_1}[\sigma'(\langle\mathbf{W}_1,\mathbf{x}\rangle))\sigma'(\langle\mathbf{W}_1,\mathbf{x}'\rangle)]\mathbf{E}_{\mathbf{W}_2}[\sigma(\langle\mathbf{W}_2,\mathbf{x}\rangle))\sigma(\langle\mathbf{W}_2,\mathbf{x}'\rangle)]\mathbf{E}_{\mathbf{W}_3}[\mathbf{W}_3^i\mathbf{W}_3^i] \\
&= 2\langle\mathbf{x},\mathbf{x}'\rangle\kappa_{\mathbf{1}}(\mathbf{x},\mathbf{x}')\kappa_{\mathbf{2}}(\mathbf{x},\mathbf{x}').
\end{aligned} \tag{21}$$

By symmetry, we obtain with a similar term for $\mathbf{W}_2$ and their total contribution to Eq. (18) adds up to twice the term obtained for $\mathbf{W}_1$. Characterizing the kernel w.r.t $\mathbf{W}_3$ is more straightforward:

$$\partial_{\mathbf{W}_3}\mathbf{f}_{\mathbf{W}}(\mathbf{x}) = \sqrt{\frac{2}{m}}\sigma(\tilde{\alpha}(\mathbf{x})) * \sigma(\tilde{\beta}(\mathbf{x})). \tag{22}$$

Therefore, its contribution to the NTK is

$$\langle \partial_{\mathbf{W}_3}\mathbf{f}_{\mathbf{W}}(\mathbf{x}), \partial_{\mathbf{W}_3}\mathbf{f}_{\mathbf{W}}(\mathbf{x}')\rangle = \frac{2}{m}\sum_{i}^{m}\sigma(\tilde{\alpha}_i(\mathbf{x}))\sigma(\tilde{\beta}_i(\mathbf{x}))\sigma(\tilde{\alpha}_i(\mathbf{x}'))\sigma(\tilde{\beta}_i(\mathbf{x}')). \tag{23}$$

Applying the law of large numbers again, as $\lim m \to \infty$, this quantity tends to:

$$\begin{aligned}\mathbf{E}_{\mathbf{W}_1,\mathbf{W}_2\sim\mathbf{N}(\mathbf{0},\mathbf{I})}\{[\sigma(\langle\mathbf{W}_1,\mathbf{x}\rangle))\sigma(\langle\mathbf{W}_1,\mathbf{x}'\rangle)][\sigma(\langle\mathbf{W}_2,\mathbf{x}\rangle))\sigma(\langle\mathbf{W}_2,\mathbf{x}'\rangle)]\}\\ = \mathbf{E}_{\mathbf{W}_1}[\sigma(\langle\mathbf{W}_1,\mathbf{x}\rangle))\sigma(\langle\mathbf{W}_1,\mathbf{x}'\rangle)]\mathbf{E}_{\mathbf{W}_2}[\sigma(\langle\mathbf{W}_2,\mathbf{x}\rangle))\sigma(\langle\mathbf{W}_2,\mathbf{x}'\rangle)]\\ = 2\kappa_{\mathbf{2}}(\mathbf{x},\mathbf{x}')\kappa_{\mathbf{2}}(\mathbf{x},\mathbf{x}').\end{aligned} \tag{24}$$

The theorem follows by summing up $2\times$ Eq. (21) and Eq. (24).

Width Requirements

As noted previously, two-layer Π-Netneeds an the extra factor $\Omega(\sqrt{\log m})$ in terms of width, to stay close to initialization The proof is largely derived from Lemma A.6 in [23], based on ideas first noted in [1] and therefore, we just provide a rough sketch here. For simplicity, consider the set of weights $(\mathbf{W_2}, \mathbf{W_3})$ fixed at initialization, i.e. at $\mathbf{W_2^{(0)}}, \mathbf{W_3^{(0)}}$ and note the first-order Taylor expansion for the Π-Net w.r.t $\mathbf{W_1}$ as follows:

$$f_{\mathbf{W}}(\mathbf{x}) \approx f^0_{\mathbf{W}}(\mathbf{x}) = f_{\mathbf{W}^{(0)}}(\mathbf{x}) + \langle\nabla_{\mathbf{W_1^{(0)}}} f_{\mathbf{W}^{(0)}}(\mathbf{x}), \mathbf{W_1} - \mathbf{W_1^{(0)}}\rangle$$

Here $f^0_{\mathbf{W}}$ denotes the first order Taylor expansion of f at $\mathbf{W}_0$. We can then expand the RHS as:

$$\sqrt{\frac{2}{m}}\sum_j \mathbf{W}^{(0)}_{3,j}(\sigma(x^T\mathbf{W}^{(0)}_{2,j})\sigma(x^T\mathbf{W}^{(0)}_{1,j}) + \sigma(x^T\mathbf{W}^{(0)}_{2,j})\sigma'(x^T\mathbf{W}^{(0)}_{1,j})x^T(\mathbf{W}_{1,j} - \mathbf{W}^{(0)}_{1,j})).$$

Consequently, we can bound the approximation error as:

$$|f_{\mathbf{W}}(\mathbf{x}) - f^0_{\mathbf{W}}(\mathbf{x})| \leqslant \sqrt{\frac{2}{m}}\sum_j |\sigma(x^T\mathbf{W}^{(0)}_{2,j})||\mathbf{W}^{(0)}_{3,j}|(\sigma(x^T\mathbf{W}_{1,j}) - (\sigma(x^T\mathbf{W}^{(0)}_{1,j}) + \sigma'(x^T\mathbf{W}^{(0)}_{1,j})x^T(\mathbf{W}_{1,j} - \mathbf{W}^{(0)}_{1,j}))|.$$

Notice that aside from the $|\sigma(x^T\mathbf{W}^{(0)}_{2,j})|$, the error term is exactly the same as that for a standard network. Also note that $P(x^T\mathbf{W}_{2,j} \geqslant \tau) = P(\sigma(x^T\mathbf{W}_{2,j}) > \tau) \leqslant e^{-\tau^2/2}$, for $\tau > 0$ by the sub-gaussian tail bound. To ensure $|\sigma(x^T\mathbf{W}^{(0)}_{2,j})| \leqslant \tau \; \forall \; j$ with probability $1-\delta$, we use the union bound to obtain the condition on τ as $m.e^{-\tau^2/2} < \delta$. Consequently, we have that $\tau \sim \Omega(\sqrt{\log m})$, which essentially becomes an additional constant factor in the error term, over the usual error terms from the standard feed-forward network.

A.3 Proof of Theorem 2: Characterizing the Π-kernel Eigendecay

Here, we sketch the proof for the rate of eigenvalue decay for the Π-kernel, corresponding to theorem 2. We first recall some connections between spherical harmonics and Gegenbauer polynomials. In mathematics, Gegenbauer polynomials or ultraspherical polynomials $C_k^{\alpha}(t)$ are orthogonal polynomials on the interval $[-1, 1]$ with respect to the weight function $(1-x^2)^{(\alpha-1)/2}$ and generalize Legendre polynomials.

Remark: Note that we use the $C_k^{\alpha}(t)$ parametrization for the Gegenbauer polynomial, which is more prevalent in mathematical literature. By setting $\alpha = \frac{d-1}{2}$, the resulting Gegenbauer polynomial is exactly the *Legendre polynomial* of degree k in $(d+1)$ dimensions, denoted by $P_k(t)$. In machine learning related literature, the latter convention is more prevalent [4, 9].

We first have the addition formula, which states that every normalized Gegenbauer polynomial is a spherical harmonic: $\sum_{j=1}^{N(d,k)} Y_{k,j}(\mathbf{x})Y_{k,j}(\mathbf{x}') = N(d,k)C_k^{(\frac{d-1}{2})}$
Also note that for any dot product Mercer kernel K (when the data is uniform on the unit sphere), we have the Mercer's decomposition in terms of spherical harmonics take the following form:

$$\begin{aligned} K(\mathbf{x}, \mathbf{x}') &= \sum_{k=0}^{\infty} \mu_k \sum_{j=1}^{N(d,k)} Y_{k,j}(\mathbf{x})Y_{k,j}(\mathbf{x}') \\ &= \sum_{k=0}^{\infty} \mu_k N(d,k) C_k^{(\frac{d-1}{2})}(\langle \mathbf{x}, \mathbf{x}' \rangle), \end{aligned} \tag{25}$$

where μ_k are its corresponding eigenvalues, and the second equality follows from the addition formula. Now, notice that κ_1 and κ_2 are also dot-product Mercer kernels and akin to Eq. (25), we can obtain their respective decompositions in terms of Gegenbauer polynomials:

$$\begin{aligned} \langle \mathbf{x}, \mathbf{x}' \rangle \kappa_{\mathbf{1}}(\mathbf{x}, \mathbf{x}') &= \sum_{k=0}^{\infty} \mu_{1,k} N(d,k) C_k^{(\frac{d-1}{2})}(\langle \mathbf{x}, \mathbf{x}' \rangle) \\ \kappa_{\mathbf{2}}(\mathbf{x}, \mathbf{x}') &= \sum_{k=0}^{\infty} \mu_{2,k} N(d,k) C_k^{(\frac{d-1}{2})}(\langle \mathbf{x}, \mathbf{x}' \rangle). \end{aligned} \tag{26}$$

From previous results [4, 7, 9], we already know the order of the eigenvalues $\mu_{1,k}$ and $\mu_{2,k}$, under the assumption that the data samples $\{\mathbf{x}\}_{i=1}^n$ follow the uniform distribution on the unit sphere $\mathbb{S}^{d+1}$. However, direct computation of eigenvalues of the Π-kernel, $\mu_{\pi,k}$, is difficult due to the complex integrals involved. And since we are more interested in the order of $\mu_{\pi,k}$ rather than the exact value, we take an alternate approach. We express κ_π as a product of kernels and attempt to deduce the order of $\mu_{\pi,k}$ by equating polynomial coefficients on both sides. More specifically, we plug the representations in Eq. (26) into the Π-kernel expression (Eq. (8))

$$\kappa_\pi(\mathbf{x}, \mathbf{x}') = 2\Big(\sum_{k=0}^{\infty} (2\mu_{1,k} + \mu_{2,k}) N(d,k) C_k^{(\frac{d-1}{2})}(\langle \mathbf{x}, \mathbf{x}' \rangle)\Big)\Big(\sum_{k=0}^{\infty} \mu_{2,k} N(d,k) C_k^{(\frac{d-1}{2})}(\langle \mathbf{x}, \mathbf{x}' \rangle)\Big). \tag{27}$$

It is evident that on the RHS, we get a product of polynomials form. Fortunately, there exist a previous result that allows us to express the product of two Gegenbauer polynomials as a linear combination of other Gegenbauer polynomials (Equation 8 in [10])

$$C_m^{(v)}(x) C_n^{(v)}(x) = \sum_{s=0}^{\min(m,n)} \frac{m+n+v-2s}{m+n+v-s} \cdot \frac{(v)_s (v)_{m-s} (v)_{n-s}}{s!(m-s)!(n-s)!} \cdot \frac{(2v)_{m+n-s}}{(v)_{m+n-s}} \cdot \frac{(m+n-2s)!}{(2v)_{m+n-2s}} C_{m+n-2s}^{(v)}(x), \tag{28}$$

where $(v)_k$ denotes the generalized binomial coefficient, i.e $(v)_k = v(v+1)(v+2)....(v+k-1)$ and $(v)_0 = 1$.

By using this expansion, coefficients for each Gegenbauer polynomial may be identified from Eq. (27).

The first step towards obtaining the result is to simplify the coefficient in Eq. (28), for which we use Stirling's approximation ($n! \sim \sqrt{2\pi n}(\frac{n}{e})^n$). In particular, we first set $m = n = k$ (assume v is an integer for convenience and k even) and then look at coefficient of the first term $C_{2k}^{(v)}(x)$ (the $2k^{th}$ harmonic) in the summation when $s = 0$:

$$\begin{aligned} \frac{2k+v}{2k+v} \cdot \frac{(v)_0 (v)_k (v)_k}{0!(k)!(k)!} \cdot \frac{(2v)_{2k}}{(v)_{2k}} \cdot \frac{(2k)!}{(2v)_{2k}} &= \frac{(v)_k (v)_k}{(k)!(k)!} \frac{(2k)!}{(v)_{2k}} \\ = \frac{((v+k-1)!)^2}{((v-1)!(k)!)^2} \frac{(2k)!(v-1)!}{(v+2k-1)!} &= \frac{((v+k-1)!)^2}{(v-1)!((k)!)^2} \frac{(2k)!}{(v+2k-1)!} \end{aligned} \tag{29}$$

Now we apply the Stirling's approximation:

$$\begin{aligned} &\frac{((v+k-1)!)^2}{(v-1)!((k)!)^2} \frac{(2k)!}{(v+2k-1)!} \\ &\qquad \sim \frac{(v+k-1)(v+k-1)^{2(v+k-1)}}{\sqrt{v-1}(v-1)^{v-1}k(k)^{2k}} \cdot \frac{\sqrt{2k}(2k)^{2k}}{\sqrt{v+2k-1}(v+2k-1)^{v+2k-1}} \end{aligned} \tag{30}$$

Now we consider the case when $k \gg v$ or equivalently, $k \gg d$ and by setting $v = (d-1)/2$, we obtain the following simplification:

$$\begin{aligned} &\frac{(v+k-1)(v+k-1)^{2(v+k-1)}}{\sqrt{v-1}(v-1)^{v-1}k(k)^{2k}} \cdot \frac{\sqrt{2k}(2k)^{2k}}{\sqrt{v+2k-1}(v+2k-1)^{v+2k-1}} \\ &\qquad \sim \frac{(k)^{(2v+2k-1)}}{k^{2k+1}} \cdot \frac{(2k)^{2k+0.5}}{(2k)^{v+2k-0.5}} \sim (\frac{k}{2})^{v-1} \sim k^{(d/2)} \end{aligned} \tag{31}$$

Note that the decay in $\mu_{1,k}, \mu_{2,k} = \Omega(k^{-d-1})$ as per known previous results [9, 4, 7]. The contribution to the eigenvalue corresponding to the $2k^{th}$ harmonic may be estimate by matching coefficients on both sides as follows:

$$\begin{aligned} \mu_{2k}^{\Pi} &\sim 2\frac{N(d,k)^2}{N(d,2k)}(2\mu_{1,k} + \mu_{2,k})\mu_{2,k}.k^{(d/2)} \\ &\sim \frac{(k)^d (k)^d}{(2k)^d}(2\mu_{1,k} + \mu_{2,k})\mu_{2,k} \\ &\sim (k)^d \Omega(k^{-d-1})\Omega(k^{-d-1})k^{(d/2)} \\ &= \Omega((2k)^{-d/2-2}) \end{aligned} \tag{32}$$

Note that for the standard two-layer neural network kernel, we would have had $\mu_{2k} = \Omega((2k)^{-d-1})$. And for now, we only considered one term in the summation with $m = n = k$ and $s = 0$. Next, we list some results for the other summation terms in the $k \gg d$ setting:

- when $m = k, n = k + 2p, s = p$, the contribution tends to $\Omega(2k^{(-d/2-2-p)})$
- $m = k - l, n = k + l, s = 0$ the contribution is upper bounded by $\Omega(2k^{(-d/2-2)})$

Consequently, from the terms in the infinite summation, the slowest decay rate is as obtained in Eq. (32), for the $k \gg d$ setting. Since the rest of the terms are strictly positive and we know the summation is finite (since μ^{Π}_{2k} is finite), we conclude that $\mu^{\Pi}_{2k} \geqslant \Omega(2k^{(-d/2-2)})$. Setting $k = k'/2$ allows us to conclude our proof.

A.4 LEARNING SPHERICAL HARMONICS WITH Π-KERNEL

Following the setup in [9], we perform a similar experiment on learning combinations of spherical harmonics in the NTK regime. We define and initialize the Π-Net exactly as specified, with a width of 32768 neurons and using vanilla gradient descent, to approximate the kernel learning in the infinite width limit. We take $n = 1000$ samples, $\{\mathbf{x}\}_{i=1}^{n}$ from the uniform distribution on the unit sphere $\mathbb{S}^{10}$. We define our target function with integral $k \in \mathcal{K}$ as follows:

$$f^*(\mathbf{x}) = \frac{1}{N(\mathcal{K})} \sum_{k \in K} A_k P_k(\langle \mathbf{x}, \zeta_k \rangle), \tag{33}$$

where the $P_k(t)$ is the Gegenbauer polynomial with degree k, ζ_k are fixed vectors that are independently generated from uniform distribution on unit sphere in $\mathbb{R}^{10}$, and $N(\mathcal{K})$ is a suitable normalizing constant to keep the order of magnitude of the target function approximately the same for different choices of $\mathcal{K}$. As noted previously, f^* may be seen as a linear combination of spherical harmonics and we compare the error residuals during the learning process in standard vs Π-Nets in the NTK regime, for varying $\mathcal{K}$. We use a moving average of range 20 on these curves to smoothen out the heavy oscillations in the latter stages.

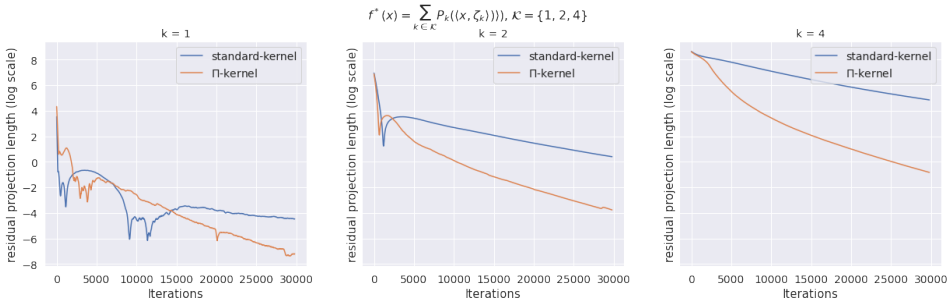

Figure 8

Figure 9: The plots represent a comparison of log-scale convergence curve of error projection lengths for standard vs Π-kernel for different order harmonics with $\mathcal{K} = \{1, 2, 4\}$, indicating a clear improvement in the rate of convergence of error for higher harmonics

For the first setting, we look at $\mathcal{K} = \{1, 2, 4\}$, with corresponding weight ratio as $A_1 : A_2 : A_4 = 1 : 1 : 1$. For each frequency, we look at the rate of convergence for the two kernels.
We observe (Fig. 9) that the rate of error convergence for the Π-kernel is much faster than the standard two-layer NTK and especially for higher harmonics (clearest increase for the highest $k = 4$), which is exactly what is expected from theoretical results.

Next, we consider $\mathcal{K} = \{1, 3, 4, 5, 8, 12\}$ i.e. we consider higher frequency harmonics and also introduce odd harmonics, with the respective A_k assigned the equal weights relative to each other. Recall that the eigenvalues corresponding to odd harmonics vanish for the standard kernel, meaning that we expect a much slower convergence rate for them. As before, we look at the rate of convergence for individual harmonics for the two kernels. The convergence curves are presented in Fig. 10. We verify the speed-up in higher frequencies, and an especially notable gap for odd harmonics other than $k = 1$.

Discussion: The empirical results strongly support our hypothesis that the Π-kernel can speed up learning higher harmonics faster than the standard two-layer kernel, even for settings outside of $k \gg d$.

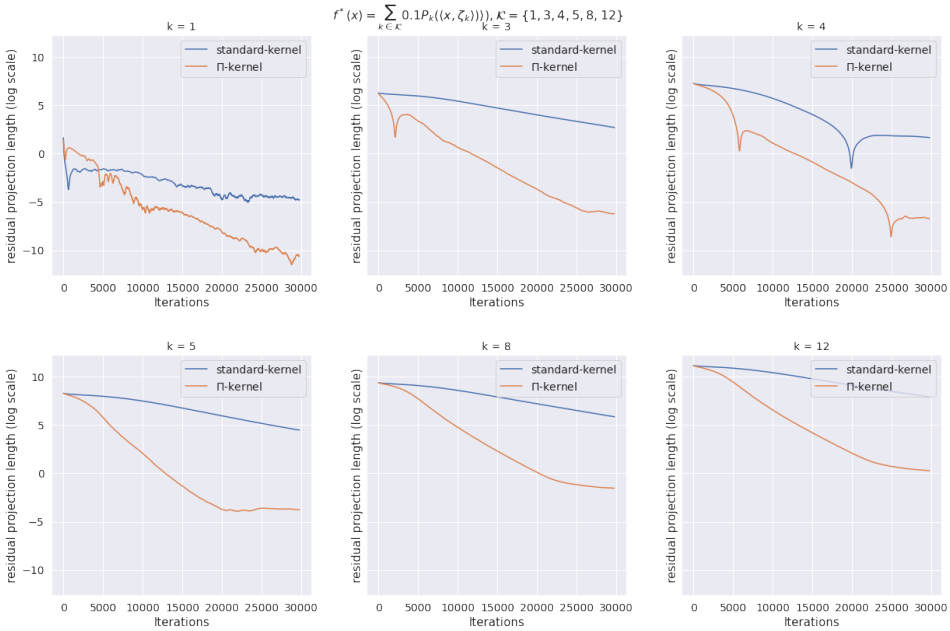

Figure 10: The plots represent a comparison of log-scale convergence curve of error projection lengths for standard vs Π-kernel for different order harmonics with $\mathcal{K} = \{1, 3, 4, 5, 8, 12\}$. We again see a clear improvement in the rate of convergence of error for higher harmonics, and especially so for odd harmonics greater than 1.

A.5 SYNTHETIC EXPERIMENTS WITH SINUSOIDS

A.5.1 ADDITIONAL EXPERIMENTS

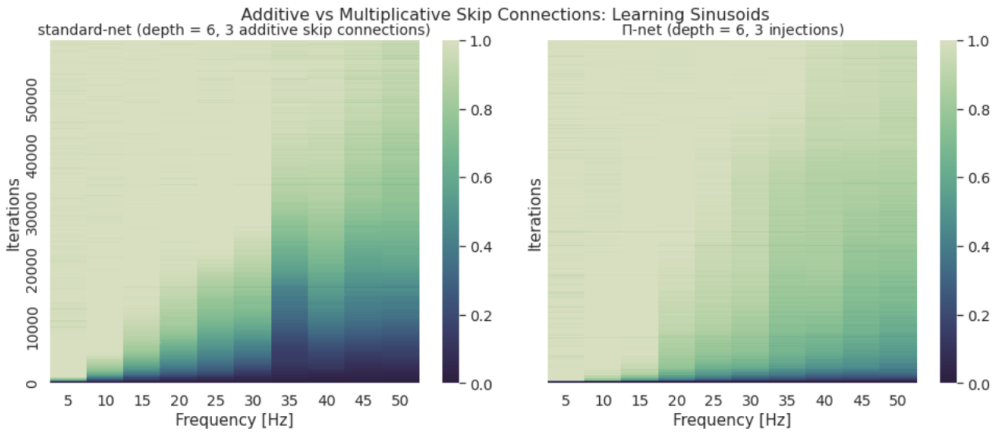

Figure 11: The heat map denotes a comparison on the effectiveness of multiplicative layers via Π-Nets vs only using additive skip connections. The additive skip connections do not seem to affect the spectral bias over standard neural networks in terms of improving speed of learning for high frequencies.

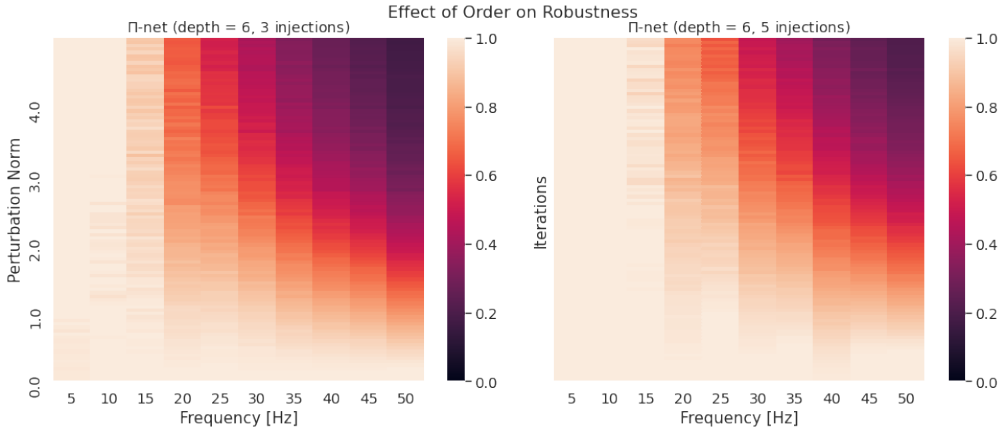

Figure 12: The heap maps present a comparison on the robustness to random parameter perturbations for two variants of Π-Nets, one with three multiplicative injection layers and the other, a higher degree polynomial with five multiplicative layers. We observe a higher degree polynomial leads to higher robustness, which is consistent with our intuition that multiplicative layers expand the solution space for learning high-frequency information.

A.6 EXPERIMENTS WITH IMAGES

A.6.1 IMPLEMENTATION DETAILS

U-net type hourglass architectures provide the ideal inductive bias for a host of image restoration tasks in the DIP framework and for our experiments, we use the same architectural design as [29] for the standard networks. Since we require the output and input to have the same spatial dimensions, the number of downsampling blocks is equal to the upsampling blocks. We refer to this number as the 'scale' of the U-net. We provide a schematic illustration in Fig. 13.

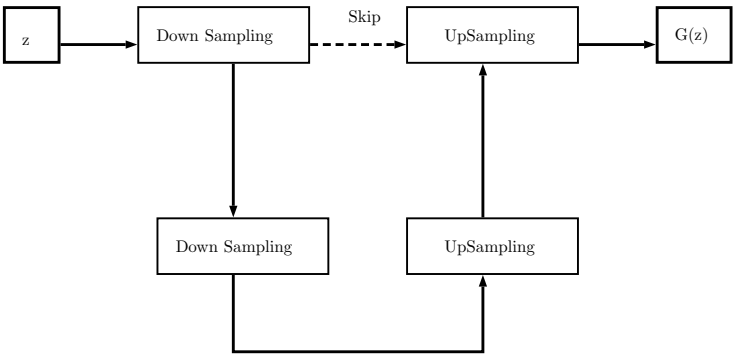

Figure 13: Illustration for the U-net with scale = 2, i.e the standard network with two upsampling/downsampling operations.

Note that the each down/upsampling block within itself contains convolutions, normalization and pooling but we abstract those details from the schematic for clarity. For the Π-network architecture, we consider a product of two polynomials model which modifies the standard network by introducing multiplicative connections. An illustrative schematic is presented in Fig. 14.

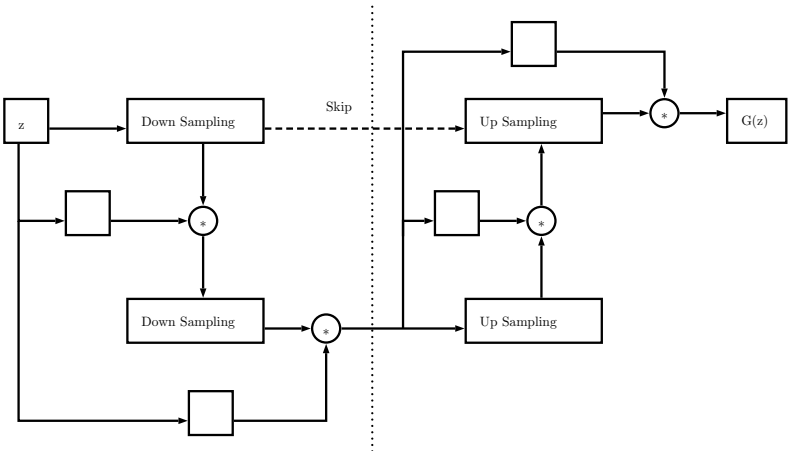

Figure 14: Adapting the 2-scale U-net for the product of two polynomials Π-network, the vertical dotted line highlights the separation between the polynomials.

Remark: In addition to the architecture, it is important to note another important detail about using Π-Nets. In practice, we recommend the use of two separate learning rates while training Π-Nets, wherein the learning rate for multiplicative connection parameters specifically is lower than the learning rate corresponding the parameters in the feed-forward part of the network. It leads to more stability while training.

A.6.2 ADDITIONAL EXPERIMENTS

(a)

(b)

Figure 15: Visual comparison of the denoised image pertaining to the denoising experiment in 4.2. We compare a snapshot (right) of the respective network outputs after 2500 iterations against the true image (left) for (a) standard network (b) Π-Net. We visually confirm that Π-network has already begun to fit the high-frequency noise faster and to a larger extent.

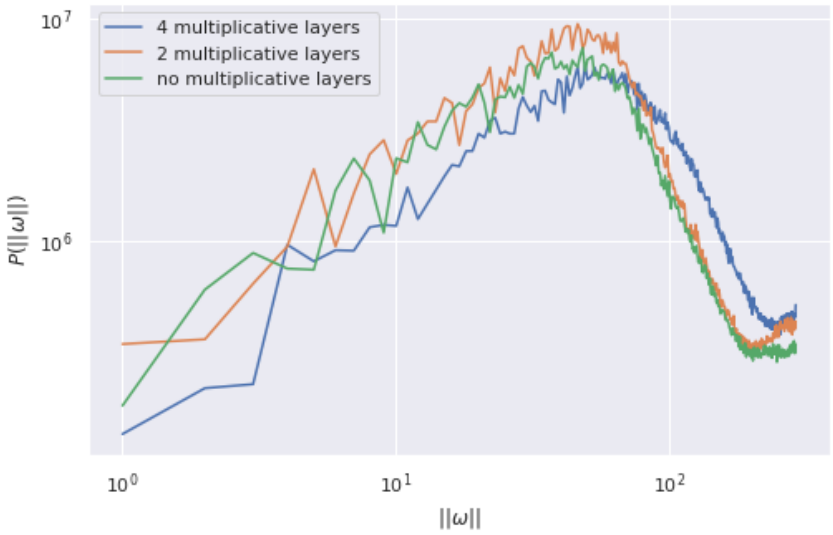

Figure 16: We visualize the deep image prior of different Π-Nets at initialization with random weights for the same input, by looking at the power spectral density of the output. With a fixed U-net architecture, introducing more multiplicative interactions in network shifts the network spectrum towards higher frequencies, which offers intuition towards understanding why multiplicative interactions speed up learning in high-frequency information.

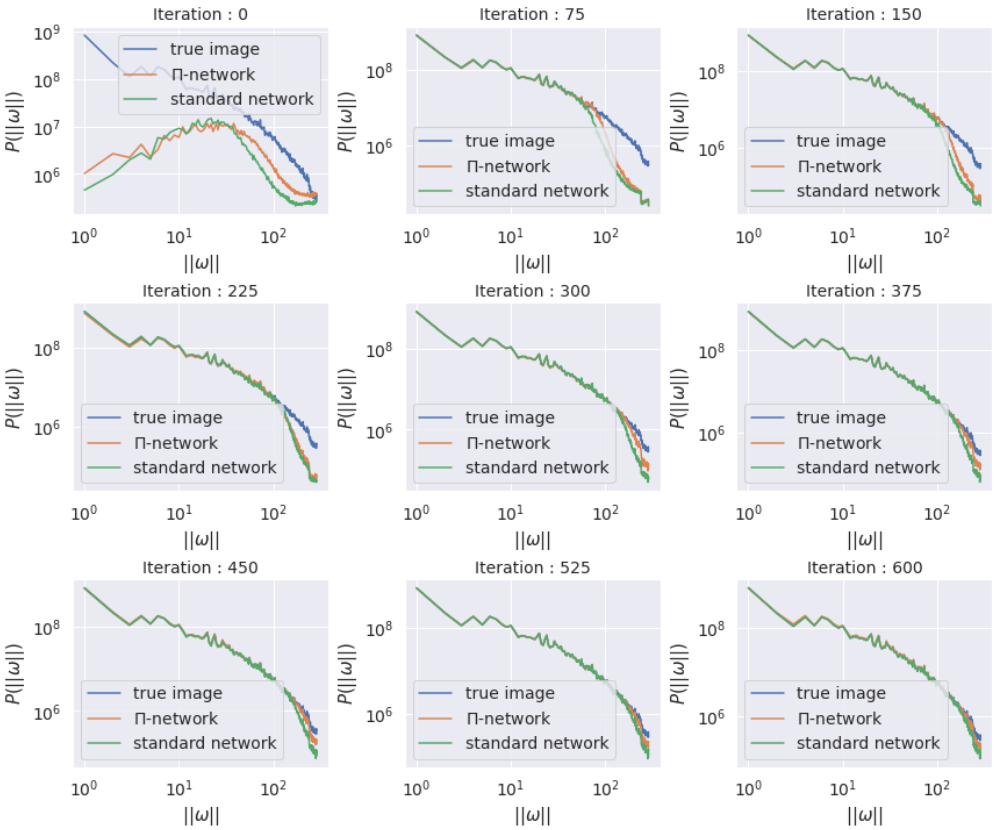

Figure 17: Comparison of the power spectral density curves over 600 iterations for standard vs Π networks (same scale) against the ground truth. We observe that the Π-Net pick up higher frequencies faster.